

Photoemission study of the skutterudite compounds $\text{Co}(\text{Sb}_{1-x}\text{Te}_x)_3$ and RhSb_3

H. Ishii, K. Okazaki, and A. Fujimori

Department of Physics and Department of Complexity Science and Engineering, University of Tokyo, Bunkyo-ku, Tokyo 113-0033, Japan

Y. Nagamoto and T. Koyanagi

Department of Symbiotic Environmental Systems Engineering, Graduate School of Science and Engineering, Yamaguchi University, Ube 755-8611, Japan

J. O. Sofo

Centro Atómico Bariloche and Instituto Balseiro, Comisión Nacional de Energía Atómica, (8400) Bariloche, RN, Argentina (November 13, 2018)

We have studied the electronic structure of the skutterudite compounds $\text{Co}(\text{Sb}_{1-x}\text{Te}_x)_3$ ($x = 0, 0.02, 0.04$) by photoemission spectroscopy. Valence-band spectra revealed that Sb $5p$ states are dominant near the Fermi level and are hybridized with Co $3d$ states just below it. The spectra of p -type CoSb_3 are well reproduced by the band-structure calculation, which suggests that the effect of electron correlations is not strong in CoSb_3 . When Te is substituted for Sb and n -type carriers are doped into CoSb_3 , the spectra are shifted to higher binding energies as predicted by the rigid-band model. From this shift and the free-electron model for the conduction and valence bands, we have estimated the band gap of CoSb_3 to be 0.03-0.04 eV, which is consistent with the result of transport measurements. Photoemission spectra of RhSb_3 have also been measured and revealed similarities to and differences from those of CoSb_3 .

PACS numbers: 79.60.-i, 72.15.Jf, 71.20.-b

I. INTRODUCTION

The family of compounds called skutterudites, with the general chemical formula TX_3 ($T = \text{Co}, \text{Rh}, \text{Ir}; X = \text{pnictogen P, As, Sb}$), have recently received much attention due to their potential for thermoelectric applications.^{1,2} The ability of thermoelectric materials is defined as the thermoelectric figure of merit,

$$Z = \frac{S^2 \sigma}{\kappa_e + \kappa_l} \propto \frac{m^{*3/2} \mu}{\kappa_l}, \quad (1)$$

where S is the Seebeck coefficient, σ is the electrical conductivity, κ_e is the electronic thermal conductivity, κ_l is the lattice thermal conductivity, m^* is the effective mass, and μ is the carrier mobility. Among the skutterudite compounds, CoSb_3 has attracted particular attention because it has a high carrier mobility (for p -type) and a heavy effective mass (for n -type).³⁻⁵ Band-structure calculations have been performed by several groups. Singh and Pickett⁶ suggested that its linear band dispersion near the Fermi level (E_F) causes the unusual transport properties. On the other hand, Sofo and Mahan⁷ reported that its band structure is typical of a narrow gap semiconductor. Moreover, Jung *et al.*⁸ proposed the chemical picture that the top of the valence band at the Γ point in the Brillouin zone corresponds to the antibonding combinations of the π_4 orbitals of the Sb ring along a crystallographic axis. It is also reported that the effective mass of the conduction band in the band-structure

calculations⁷ is nearly by a factor of ten smaller than that estimated from the transport experiments,⁴ which may indicate the existence of some effects not described by the conventional band picture. X-ray photoemission (XPS) experiments on CoAs_3 , CoSb_3 and RhSb_3 were performed⁹, but the energy resolution was not sufficient to investigate the electronic structures near E_F . Therefore, it is important to perform a photoemission study of CoSb_3 with higher energy resolution.

In this paper, we report on the results of a photoemission study of $\text{Co}(\text{Sb}_{1-x}\text{Te}_x)_3$ ($x = 0, 0.02, 0.04$) including ultraviolet photoemission spectroscopy (UPS). First, we show the valence-band spectra of CoSb_3 ($x = 0$), which were taken with much higher resolution than in the previous reports,⁹ and revealed that Sb $5p$ orbitals are indeed dominant near E_F in CoSb_3 . Second, we compare the valence-band spectra of CoSb_3 with a theoretical spectrum derived from the band-structure calculation.⁷ The photoemission spectra are well reproduced by the theoretical spectrum, which suggests that the effect of electron correlations is not strong in CoSb_3 . Third, we show a rigid-band like spectral shift in $\text{Co}(\text{Sb}_{1-x}\text{Te}_x)_3$ ($x = 0, 0.02, 0.04$) as a function of x . From the spectral shift we have estimated a band gap of CoSb_3 to be 0.03-0.04 eV. We also compare the spectra of CoSb_3 with those of RhSb_3 and discuss the differences between them. Finally, the temperature dependence of the spectra near E_F have been studied and have revealed unusual behaviors in both compounds.

II. EXPERIMENT

Samples of $\text{Co}(\text{Sb}_{1-x}\text{Te}_x)_3$ ($x = 0, 0.02, 0.04$) were prepared by the following method. Co (99.998% pure), Sb (99.9999% pure) and Te (99.9999% pure) powders were used as starting materials. They were mixed in stoichiometric ratio $\text{Co}(\text{Sb}_{1-x}\text{Te}_x)_3$ ($x = 0, 0.02, 0.04$) in a plastic vial before being loaded in a steel die, where they were compressed into a dense cylindrical pellet. The pellet was loaded on a graphite boat in an Ar atmosphere, which was heated for two days at 823 K. The product was then crushed and ground in an alumina mortar. Following the powder reaction, several samples of $\text{Co}(\text{Sb}_{1-x}\text{Te}_x)_3$ were sintered by the spark plasma sintering method. The spark plasma sintering was performed under a pressure of 30 MPa at 853 K for 10 min. CoSb_3 was single-crystalline and showed *p*-type transport, while $\text{Co}(\text{Sb}_{0.98}\text{Te}_{0.02})_3$ and $\text{Co}(\text{Sb}_{0.96}\text{Te}_{0.04})_3$ were polycrystalline and showed *n*-type transport.

We performed the photoemission experiments using a hemispherical electron energy analyzer. The light sources were the He I ($h\nu = 21.2$ eV) and He II ($h\nu = 40.8$ eV) resonance lines for UPS, and the Mg $K\alpha$ ($h\nu = 1253.6$ eV) line for XPS. Energy calibration and estimation of the instrumental resolution were done for Au film evaporated on the samples after each series of measurements. The energy resolution was about 25 meV, 100 meV and 0.7 eV for He I UPS, He II UPS and XPS, respectively. Measurements were done at 30 K, 100 K and 300 K for He I, and only at 300 K for He II and XPS. The base pressure in the spectrometer was $\sim 1 \times 10^{-10}$ Torr for UPS and $\sim 5 \times 10^{-10}$ Torr for XPS. The surfaces of the samples were repeatedly scraped *in situ* with a diamond file. When they were scraped at low temperatures ($T < 100$ K), however, the structures caused by the adsorption of impurity were observed in the photoemission spectra. Therefore, we measured only 30 K spectra after scraping at 100 K and lowering the temperature down to 30 K.

III. RESULTS AND DISCUSSION

Figure 1(a) and (b) show the valence-band photoemission spectra of CoSb_3 in the entire valence-band region and in the vicinity of E_F , respectively, at various photon energies. Roughly speaking, four structures are distinguishable in the spectra. Here, these structures are referred to as *A* (from 0 to 2 eV), *B* (from 2 to 3.3 eV), *C* (from 3.3 to 6 eV) and *D* (from 7.5 to 12 eV) as indicated in the figure. Based on the fact that the relative cross-section of Sb 5*p* to Co 3*d* is the smallest at $h\nu = 40.8$ eV,¹⁰ one can make the following assignment of the spectral features. The distinct peak of *A* is assigned to be mainly of Co 3*d* character because it is strong in all the spectra. Peak *A* consists of two structures, *a* and *b*, as indicated in Fig. 1. *a* is observed both in the He I

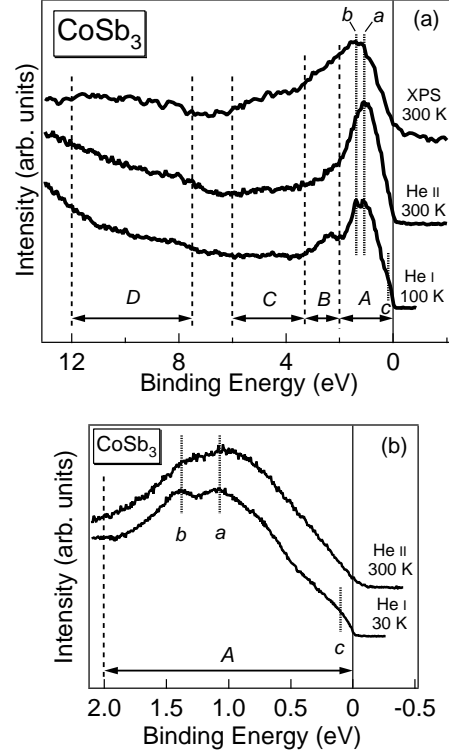


FIG. 1. Valence-band photoemission spectra of CoSb_3 in the entire valence-band region (a) and in the vicinity of E_F (b).

and He II spectra, while *b* is hardly observed in the He II spectrum. Judging from the relative cross-section of Sb 5*p* to Co 3*d*,¹⁰ one can assign *a* to relatively pure Co 3*d* character and *b* to Co 3*d* states hybridized with Sb 5*p* states. Moreover, a small hump denoted by *c* is observed in the region between 0 and 0.3 eV in the He I spectrum and not in the He II spectrum. In a similar way to *b*, we assign this hump to Sb 5*p* character. These results indicate that the valence-band maximum has predominantly Sb 5*p* character, consistent with the results of the previous band-structure calculations.⁶⁻⁸ Structures *B* and *C* can be assigned to Sb 5*p* character, because they are observed in the He I and XPS spectra but not in the He II spectrum. According to the band-structure calculation,⁷ Sb 5*p* has a broad structure in the region between E_F and 6 eV, and therefore *C* is part of the broad structure. On the other hand, *B* includes Co 3*d* character, too, because, when we substitute Rh for Co, *C* does not change its binding energy, but *B* changes its binding energy together with *A*, as described below (Fig. 5). One can assign structure *D* to Sb 5*s* character, because it increases with photon energy, which is consistent with the fact that the relative cross-section of Sb 5*s* to Co 3*d* increases with photon energy.¹⁰

In Fig. 2, we make a quantitative comparison between

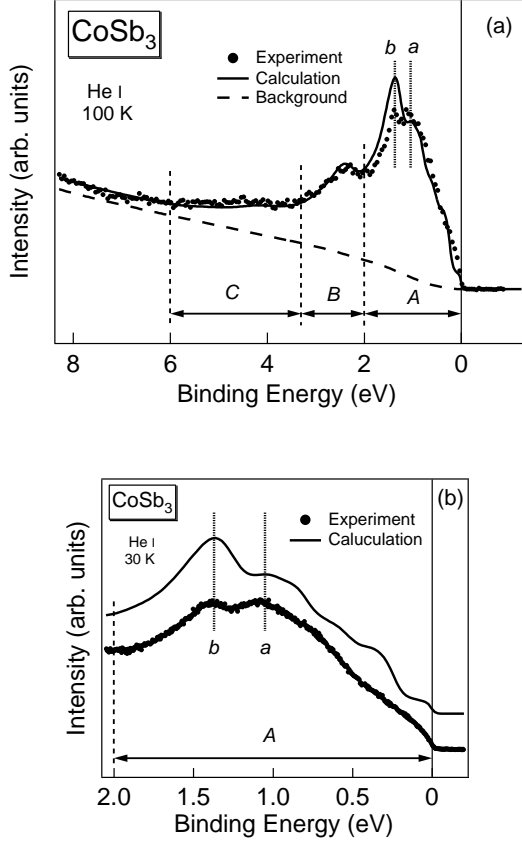


FIG. 2. Photoemission spectra of CoSb_3 compared with the band-structure calculation⁷ in the entire valence-band region (a) and in the vicinity of E_F (b). The dashed curve shows the background (see text). The spectra have been normalized to the area between E_F and 6 eV.

the He I photoemission spectrum and the theoretical spectrum derived from the band-structure calculation by Sofo and Mahan.⁷ To derive the theoretical photoemission spectrum we have taken into account the contribution of the Co 3*d*, Sb 5*s* and Sb 5*p* partial density of states (DOS). They have been weighted by the corresponding photoionization cross-sections at that photon energy.¹⁰ This weighted DOS has been broadened by convoluting with a Gaussian and a Lorentzian which represent the instrumental resolution and the lifetime broadening, respectively. We assume that the lifetime width increases linearly with energy E measured from E_F , i.e., $\text{FWHM} = \alpha|E - E_F|$. The coefficient α , which represents the lifetime of the photo-hole and increases with increasing binding energy, is empirically determined to be ~ 0.1 . Finally, we have added the background of Hemrich type¹¹ to the broadened DOS, as shown by a dashed line in Fig. 2(a). The spectra have been normalized to the area between E_F and 7 eV.

In the wide energy range [Fig. 2(a)], the photoemis-

TABLE I. Values for the Fermi energy ϵ_F , the effective mass m^* , and the carrier concentration n . The values of m^* are taken from Ref. 4 and m_e is the free-electron mass.

	type	ϵ_F [eV]	m^*	n [cm ⁻³]
CoSb_3	<i>p</i>	0.03	$0.15 \times m_e$	1.4×10^{18}
$\text{Co}(\text{Sb}_{0.96}\text{Te}_{0.04})_3$	<i>n</i>	0.06	$3.5 \times m_e$	4×10^{20}

sion spectrum is in good agreement with the theoretical spectrum. The main structures, A, B, and C, which were defined in Fig. 1, are well reproduced in the theoretical simulation. These results suggest that electron correlations are not important in CoSb_3 . However, there exists a small discrepancy in the fine structures in A between the photoemission spectrum and the theoretical spectrum. The intensity ratio b/a is different between experiment and calculation. The intensity of b is as high as that of a in the photoemission spectrum, while it is apparently higher than that of a in the theoretical spectrum. As mentioned above, a and b can be assigned to relatively pure Co 3*d* and Co 3*d* states hybridizing with Sb 5*p* states, respectively. The local-density approximation used for the band-structure calculation tends to overestimate the hybridization between the Co 3*d* and Sb 5*p* electrons, and hence the hybridization strength may have been overestimated.

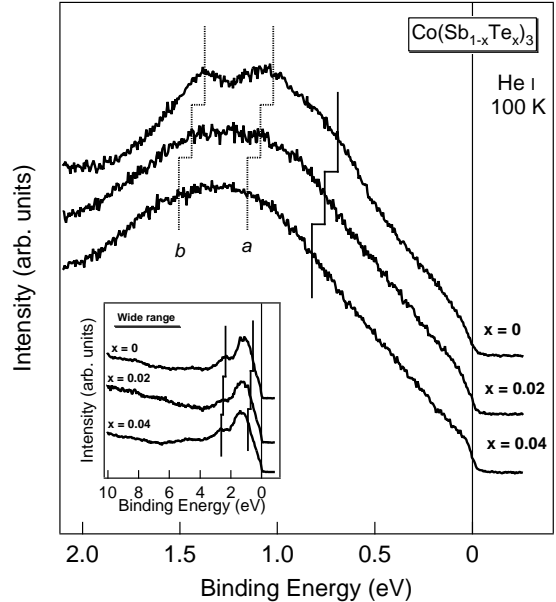


FIG. 3. Photoemission spectra of $\text{Co}(\text{Sb}_{1-x}\text{Te}_x)_3$ ($x = 0, 0.02, 0.04$) near E_F . The inset shows wide-range spectra. The spectra have been normalized to the height of the Co 3*d* peak.

Figure 3 shows the valence-band spectra

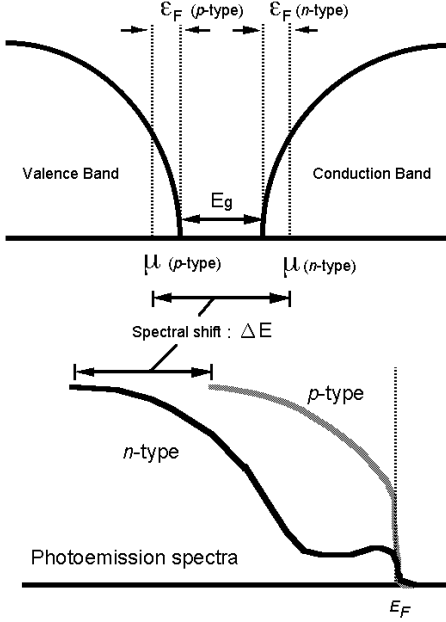


FIG. 4. Schematic illustration of the spectral DOS for p -type and n -type semiconductors, which is observed by photoemission spectroscopy.

of $\text{Co}(\text{Sb}_{1-x}\text{Te}_x)_3$ in the vicinity of E_F . The spectra have been normalized to the height of the peak at ~ 1.2 eV. The spectra of the $x = 0.02$ and $x = 0.04$ samples are more blurred than the $x = 0$ sample, probably because the substitution of Te for Sb caused potential disorder in the crystal. Energy shifts of them were determined by comparing the positions of the low binding energy side of the Co $3d$ peak, as indicated by a solid line in the figure. The spectra of $\text{Co}(\text{Sb}_{1-x}\text{Te}_x)_3$ are shifted to higher binding energy with increasing x . This is what would be expected from the rigid-band model since Te has one more valence electron than Sb and hence each substituted Te atom donates one electron to the conduction band. We obtained the spectral shifts of 0.05-0.06, 0.06-0.07, and 0.12-0.13 eV for $x = 0 \rightarrow 0.02$, $x = 0.02 \rightarrow 0.04$, and $x = 0 \rightarrow 0.04$, respectively. From these shifts we estimated the band gap of CoSb_3 as follows. The $x = 0$ and $x = 0.04$ samples are p -type and n -type degenerate semiconductors, respectively, and their chemical potentials are located below the valence-band maximum for the p -type material and above the conduction-band minimum for the n -type material, as illustrated in Fig. 4. In the regions between μ and the band edge, one can regard the energy band to be parabolic. Then the separation between μ and the band edge corresponds to the Fermi energy ϵ_f of the carriers and is given by:

$$\epsilon_f = \frac{\hbar^2 k_F^2}{2m^*}, \quad (2)$$

where k_F and m^* are the Fermi wave vector and the

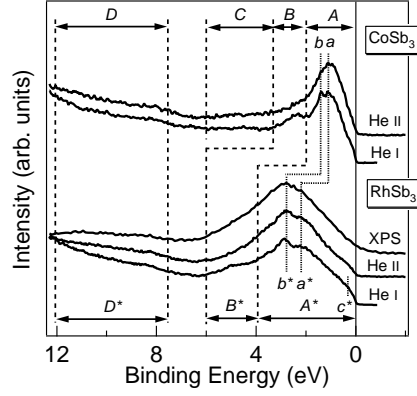


FIG. 5. Photoemission spectra of RhSb_3 compared with those of CoSb_3 .

effective mass of the carriers, respectively. k_F is given by:

$$k_F = (3\pi^2 n)^{1/3}, \quad (3)$$

where n is the carrier concentration. The values of ϵ_f , k_F , m^* , and n in the measured samples are listed in Table I. Here, we used the room temperature values of n , because the values at room temperature are little different from those at 100 K in the case of degenerate semiconductors. In the photoemission spectra, the binding energy corresponds to the energy difference from μ . When electrons are doped and μ rises, the spectra are shifted to higher binding energies, as illustrated in Fig. 4. In this way, one can estimate the band gap E_g from the measured shift ΔE as:

$$E_g = \Delta E - \epsilon_{F(x=0)} - \epsilon_{F(x=0.04)} \quad (4)$$

and obtains the value of 0.03-0.04 eV for E_g . This value is consistent with the value of $E_g \sim 0.05$ eV deduced from the transport experiments^{3,4,12} within the experimental uncertainties.

Figure 5 shows the valence-band photoemission spectra of RhSb_3 . In analogy to CoSb_3 , we refer to the main structures as A^* (from 0 to 4 eV), B^* (from 4 to 6 eV) and D^* (from 7 to 12 eV) as indicated in the figure, corresponding to A , B and D in the CoSb_3 spectra. Structure C^* , which should correspond to C , is not observed, probably because it is hidden by A^* and B^* , which are located at higher binding energies and are broader than those in CoSb_3 . Moreover, fine structures a^* , b^* and c^* within A^* are also defined as indicated in the figure. As in the case of CoSb_3 , structure A^* is assigned to Rh $4d$. A^* is broader than A , which indicates that the Rh $4d$ band is wider than the Co $3d$ band. Moreover, the intensity ratio b^*/a^* is different from b/a of CoSb_3 . For CoSb_3 , b is as strong as a in the He I spectrum and is much weaker than a in the He II spectrum. On the other hand, for RhSb_3 ,

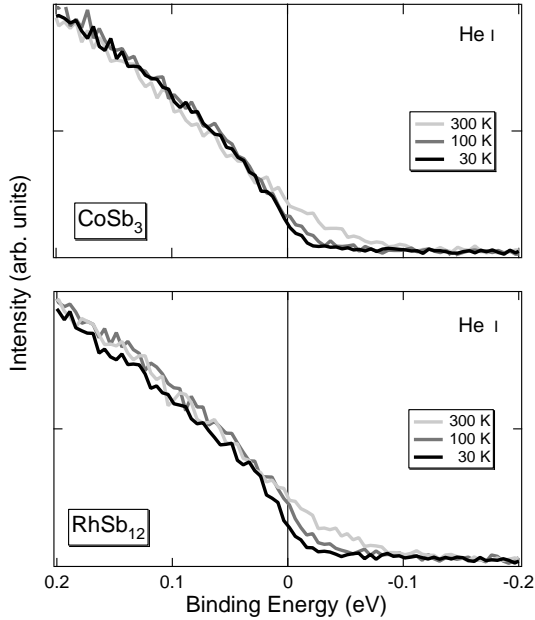


FIG. 6. Temperature-dependent photoemission spectra of CoSb₃ and RhSb₃ in the region near E_F . The spectra have been normalized to the area between -0.2 and 2 eV for CoSb₃, and between -0.2 and 4 eV for RhSb₃.

b^* is stronger than a^* both in the He I and He II spectra, although the intensity ratio b^*/a^* is slightly smaller in the He II spectrum. One can explain these differences as follows. From the results of the CoSb₃ spectra, we can regard a^* as pure d character and b^* as hybridized d character. Since Rh 4d electrons are more itinerant than Co 3d electrons, b^*/a^* for RhSb₃ is larger than CoSb₃. The hump just below E_F , c^* , is also identified in RhSb₃ and can be assigned to Sb 5p states. Structures B^* and D^* are assigned to Sb 5p character and to Sb 5s character, respectively, in the same way as B and D . Comparing the RhSb₃ spectra with the CoSb₃ spectra, B^* is located at a higher binding energy than B in the same way as A^* (A), which is of d character. On the other hand, structures D^* is located at the same binding energies as D . C^* is probably hidden by B^* and, if this is the case, it is located at the same energy as C . These results suggest that B^* (B) hybridizes with d states and that C^* (C) does not.

Finally, Fig. 6 shows the temperature-dependent spectra of CoSb₃ and RhSb₃ in the region near E_F . The spectra have been normalized to the area between -0.1 and 2 eV for CoSb₃ and between -0.1 and 4 eV for RhSb₃. One can see that the intensities of the spectra around E_F decrease with decreasing temperature. To isolate the temperature dependence of the spectral DOS from the temperature dependence of the Fermi-Dirac (FD) distribution function, we have divided the spectra by the FD distribution function (convoluted with a Gaussian cor-

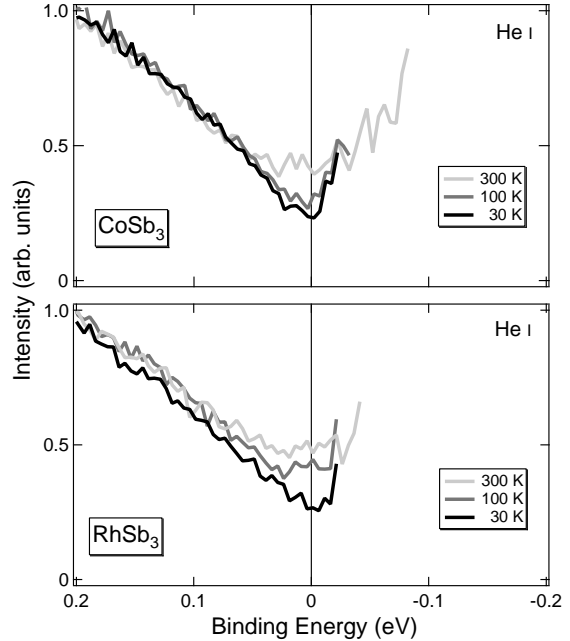


FIG. 7. Temperature-dependent spectral DOS, which have been obtained by dividing the spectra in Fig. 6 by the Fermi Dirac distribution function.

responding to the instrumental resolution)^{13,14} as indicated in Fig. 7. In the figure, we find in each spectrum the formation of a dip in the DOS at E_F , which becomes deeper with decreasing temperature. The magnitudes of these dips (pseudogaps) are ~ 0.05 and ~ 0.1 eV for CoSb₃ and RhSb₃, respectively. These results may indicate spectral weight transfer over large energies of order eV. This anomalous temperature dependence near E_F cannot be explained by the simple band picture. Here we may suggest two candidates which can cause the above phenomena. First, we may consider electron-electron interaction between the Sb 5p electrons forming the anti-bonding combinations of the π_4 orbitals of the Sb ring, which was reported by Jung *et al.*⁸ This possibility is, however, rather unlikely because of the itinerant nature of the Sb 5p electrons. Second, electron-phonon interactions may be considered. It has been reported that the most prominent lines in Raman spectra of CoSb₃ and RhSb₃ are due to the Sb₄-ring breathing modes and their energy is ~ 0.02 eV,¹⁵ which may modulate the electronic states around the valence-band maximum with decreasing temperature from 300 K. Indeed, Sofo and Mahan⁷ reported that small changes in the positions of the Sb atoms affect strongly the electronic structures near E_F . Further studies are necessary to elucidate the origin of the unusual observations.

IV. CONCLUSION

We have performed the photoemission study of $\text{Co}(\text{Sb}_{1-x}\text{Te}_x)_3$ ($x = 0, 0.02, 0.04$) and RhSb_3 . The top of the valence band of CoSb_3 is of Sb $5p$ character hybridized with Co $3d$ state just below it. The photoemission spectra of CoSb_3 were well reproduced by the band-structure calculation⁷, which suggests that electron correlation does not play an important role in the electronic structure of CoSb_3 . When Te is substituted for Sb and electrons are doped into CoSb_3 , the photoemission spectra are rigidly shifted to higher binding energies. From this spectral shift, we have estimated the band gap of CoSb_3 to be 0.03-0.04 eV, which is consistent with the transport experiments.^{3,4,12} The spectra of RhSb_3 are similar to CoSb_3 to some extent, whereas some differences are caused by the wider band width of Rh $4d$. Unusual temperature-dependence has been observed for the spectra of CoSb_3 and RhSb_3 in the region near E_F , which we tentatively attribute to the effect of Sb_4 -ring breathing phonons.

V. ACKNOWLEDGMENT

The authors would like to thank T. Susaki, J. Matsuno and A. Chainani for their useful discussions. One of us J. O. S. is supported by CONICET Argentina.

- ¹⁰ J.-J. Yeh and I. Lindau, *At Data Nucl. Data Tables* **32**, 1 (1985).
- ¹¹ X. Li, Z. Zhang, and V. E. Henrich, *J. Electron Spectrosc. Relat. Phenom.* **63**, 253 (1993).
- ¹² E. Arushanov, M. Respaud, H. Rakoto, J. M. Broto, and T. Caillat, *Phys. Rev. B* **61**, 4672 (2000).
- ¹³ T. Susaki, Y. Takeda, M. Arita, K. Mamiya, A. Fujimori, K. Shimada, H. Namatame, M. Taniguchi, N. Shimizu, F. Iga, and T. Takabatake, *Phys. Rev. Lett.* **82**, 992 (1999).
- ¹⁴ H. Kumigashira, T. Sato, T. Yokota, T. Takahashi, S. Yoshii, and M. Kasuya, *Phys. Rev. Lett.* **82**, 1943 (1999).
- ¹⁵ G. S. Nolas, G. A. Slack, T. Caillat, and G. P. Meisner, *J. Appl. Phys.* **79**, 2622 (1996).

-
- ¹ B. C. Sales, D. Mandrus, and R. K. Williams, *Science* **272**, 1325 (1996).
 - ² J.-P. Fleurial, T. Caillat, A. Borshchevsky, D. T. Morelli, and G. P. Meisner, in *Proceedings of the 15th International Conference on Thermoelectrics*, edited by T. Caillat (Institute of Electrical and Electronics Engineers, Piscataway, New Jersey, 1996), p. 91.
 - ³ D. Mandrus, A. Migliori, T. W. Darling, M. F. Hundley, E. J. Peterson, and J. D. Thompson, *Phys. Rev. B* **52**, 4926 (1995).
 - ⁴ T. Caillat, A. Borshchevsky, and J.-P. Fleurial, *J. Appl. Phys.* **80**, 4442 (1996).
 - ⁵ D. T. Morelli, T. Caillat, J.-P. Fleurial, A. Borshchevsky, and J. Vandersande, B.Chen, and C. Uher, *Phys. Rev. B* **51** 9622 (1995).
 - ⁶ D. J. Singh and W. E. Pickett, *Phys. Rev. B* **50**, 11 235 (1994).
 - ⁷ J. O. Sofo and G. D. Mahan, *Phys. Rev. B* **58**, 15 620 (1998).
 - ⁸ Dongwoon Jung, Myung-Hwan Whangbo, and Santiago Alvarez, *Inorg. Chem.* **29**, 2252 (1990).
 - ⁹ H. Anno, K. Matsubara, T. Caillat, and J.-P. Fleurial, *Phys. Rev. B* **62** 10 737 (2000).